arXiv:1509.00101v1 [cond-mat.str-el] 1 Sep 2015

Quantum Spin Fluctuations and magnons in antiferromagnetically coupled bilayers with tuneable intra-bilayer exchange - the case of $Cr_2W(Te)O_6$

Kingshuk Majumdar[*]
Department of Physics, Grand Valley State University, Allendale, Michigan 49401, USA

S. D. Mahanti[†]
Department of Physics and Astronomy,
Michigan State University, East Lansing, Michigan 48824, USA

(Dated: September 2, 2015)

Abstract

Recent neutron diffraction studies have shown that in $Cr_2(W,Te)O_6$ systems, which consist of bilayers with strong antiferromagnetic inter-bilayer coupling between Cr moments, the intra-bilayer coupling between the Cr moments can be tuned from ferro (for W) to antiferro (for Te). *Ab initio* density functional calculations provide a microscopic understanding of the magnetic structure but cannot explain the magnitude of the ordered Cr^{3+} moments. In order to understand the reduction of the ordered moment caused by quantum spin fluctuations (QSF) we have studied the magnon dispersion and the sublattice magnetization using a two parameter quantum Heisenberg spin Hamiltonian with tunable intra-(j) and antiferromagnetic inter- (J) bilayer couplings. In the $j = 0$ limit the system reduces to decoupled quantum dimers. The magnon dispersion and normalized sublattice magnetization (NSM) have been calculated using non-linear spin wave theory up to second-order corrections ($1/S^2$) in spin S. The effect of J is quite dramatic when j is ferromagnetic, a large peak in magnon dispersion appears at the corner of the Brillouin zone for large J (realistic case) in addition to changing the quadratic dispersion to linear. Inelastic neutron scattering experiments can confirm this theoretical prediction. The effect of J on NSM is simple when j is ferromagnetic, NSM decreases monotonically with J. In contrast when j is antiferromagnetic the effect of J is to suppress QSF effect until $J \sim j$ but further increase in J gives rise to increasing QSF reduction of the NSM. These theoretical results are qualitatively consistent with experiment.

PACS numbers: 71.15.Mb, 75.10.Jm, 75.25.-j, 75.30.Et, 75.40.Mg, 75.50.Ee, 73.43.Nq

I. INTRODUCTION

Quantum spin fluctuations (QSF) play an important role in the low temperature properties of quantum antiferromagnets (QAF), particularly in systems with low spin and low dimension.[1–4] For example, the ordered moment or sublattice magnetization (M_s) in a nearest-neighbor (NN) D-dimensional spin-1/2 Heisenberg quantum antiferromagnet (HQAF) is zero for $D = 1$ (no long range order), $0.3067\mu_B$ for $D = 2$[1,5] and $0.423\mu_B$ for $D = 3$ (isotropic couplings)[6], the latter two values obtained in a leading order approximation (to be discussed later in the paper). Thus QSF decrease with increasing S and increasing D. The interplay of QSF and covalency induced reduction of M_s in QAFs has also been a subject of great interest in the past, particularly in the parent compound of high T_c superconductors (La_2CuO_4 where the Cu^{2+} ions have $S = 1/2$, form a square lattice and interact with NN isotropic Heisenberg AF interaction).[7]

Recently Zhu et al[8] have studied the magnetic structure of an interesting class of layered magnetic systems containing Cr^{3+} (d^3 configuration - spin 3/2) where the magnetic ions are arranged in bilayers. The inter-bilayer coupling is strongly antiferromagnetic due to the presence of Cr^{3+}-Cr^{3+} dimers with strong intra-dimer AF couplings. The intra-bilayer couplings however can be either AF or ferromagnetic (F) depending on whether the system contains Te or W (also Mo) atom.[9] In fact the average intra-bilayer exchange can be tuned from one limit to the other in $Cr_2W_{1-x}Te_xO_6$ by changing x from 0 to 1. Neutron powder diffraction (NPD) measurements have determined the ground state spin structure and the values of the sublattice magnetization. The Te compound consists of antiferromagnetic bilayers which are coupled antiferromagnetically (AF-AF). In contrast the W and Mo analogs consist of ferromagnetic bilayers coupled antiferromagnetically (F-AF). In addition to the magnetic ordering the NPD measurements also give the values of M_s. The values of M_s are reduced from their atomic spin value $3.0\mu_B$ for Cr^{3+} ($M_s = g\mu_B S$) assuming $g = 2$ and quenched orbital angular momentum. This reduction can be due to covalency where the Cr d orbitals hybridize with O p orbitals and due to QSF.[7] Electronic structure calculations reveal information about the reduction due to covalency whereas QSF-caused reduction can be calculated using a Heisenberg spin Hamiltonian, which is the major focus of this paper.

Ab initio electronic structure calculations using density functional theory (GGA and GGA+U)[10–12] correctly reproduced the magnetic ordering in these three compounds.[7,8] Since the orbital angular momentum is quenched for the d^3 configuration (three electrons in the local t_{2g} orbitals; $S = 3/2$) the magnetic moment comes from the spin. The estimated exchange parameters (inter-bilayer or inter-dimer exchange J and intra-bilayer NN exchange j) were reasonable in view of the limitations of GGA or GGA+U approximations.[8] However the calculated values of the sublattice magnetization ($\sim 2.8\mu_B$) was very close to the ionic value ($3.0\mu_B$) indicating a small covalent reduction of the ordered moment.[8] In contrast, the experimental values are reduced to $\sim 2.3\mu_B$.[8] One possible reason for this reduction is QSF.[1] Such dramatic reduction in ordered moment has been seen in many quasi-two dimensional QAFs, a classic example being La_2CuO_4 which consists of antiferromagnetic $2D$ square lattice of $S = 1/2$, where QSF reduces the sublattice magnetization (M_s) by $\sim$40%.[1] In the present systems the reduction should be smaller (at least by a factor of three) due to $S = 3/2$.

To visualize the magnetic ordering and magnetic exchange in the system we will consider the ground state spin ordering in Cr_2(M=Te,W, Mo)O_6 (see Fig. 1).[13] One has two bilayers (perpendicular to the z-axis) in the tetragonal unit cell (a, a, c) and four Cr spins/unit cell. The experimental unit cell parameters are $a = 4.545$Å and $c = 8.995$Å for Cr_2TeO_6 and $a = 4.583$Å and $c = 8.853$Å for Cr_2WO_6.[8] The distance between the inter-bilayer (NN) Cr atoms i.e. Cr1 and Cr3 is $\delta \sim 3.00$Å $\approx c/3$, whereas the distance between intra-bilayer NN Cr atoms (Cr1 and Cr2 or Cr3 and Cr4) is $\sim$ 3.80Å. One bilayer contains Cr1 and Cr2 spins and the other contains Cr3 and Cr4 spins. The inter-bilayer coupling comes through Cr1-Cr3 and Cr2-Cr4 dimers, it is antiferromagnetic and its strength is denoted by J. The NN intra-bilayer coupling is between Cr3-Cr4 and Cr1-Cr2 and its strength is denoted by j. The magnitude of j is considerably smaller than that of J in these systems which can therefore regarded as weakly interacting quantum dimers, J being the strength of intra-dimer antiferromagnetic coupling. In Cr_2MoO_6 and in Cr_2WO_6 the inter-dimer (also the intra-bilayer) coupling is ferromagnetic making the bilayers ferromagnetic. On the other hand, in Cr_2TeO_6 the intra-bilayer coupling is antiferromagnetic. In thermodynamic measurements the high temperature properties (for example peak in heat capacity) are determined primarily by the dimers i.e. the energy scale is set by the intra-dimer coupling strength J whereas for the low temperature properties below the antiferromagnetic transition temperature the intra-dimer coupling j is responsible for the long range order. Also it plays an important role in magnon dispersion and quantum spin fluctuations. Experimental values of the couplings are: $J = -2.9$ meV and $j = -0.4$ meV for Cr_2TeO_6 and $J = -3.8$ meV and $j = 0.12$ meV for Cr_2WO_6.[14]

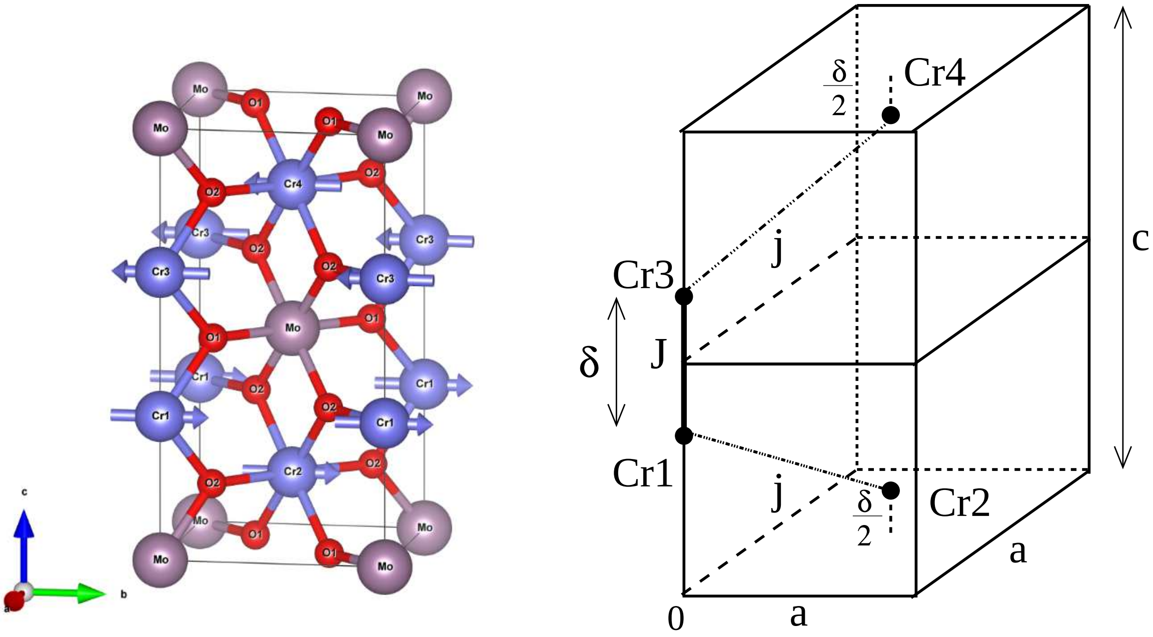

FIG. 1. (Color online)(a) Schematic of the bilayer crystal structure of Cr_2MO_6 (M=Te, W, Mo). Each Cr^{3+} bilayer is separated by a (Te, Mo, W) layer.[8,9] (b) Positions of four chromium spins in the tetragonal unit cell of dimensions (a, a, c) are shown. The coordinates of the spins are: Cr1: $(0, 0, c/2 - \delta/2)$, Cr2: $(a/2, a/2, \delta/2)$, Cr3: $(0, 0, c/2 + \delta/2)$, and Cr4: $(a/2, a/2, c - \delta/2)$. Within each bilayer Cr1 (Cr3) spin is coupled with Cr2 (Cr4) spin (shown by dashed lines with coupling strength j). On the other hand, for the inter-bilayer NN coupling Cr1 and Cr3 are coupled within the same tetragonal cell (shown by a thick solid line with coupling strength J) whereas Cr2 is coupled to Cr4 in the unit cell below and Cr4 is coupled with Cr2 in the unit cell above.

The present systems are somewhat peculiar. The inter-bilayer coupling J is AF and strong. The intra-bilayer coupling j is small and can be either F or AF. If we put $j = 0$, then the system consists of non-interacting quantum spin $S = 3/2$ dimers and the ground state consists of a product of dimer singlet states and there is no long range order (LRO). If on the other hand, $J = 0$, the system consists of non-interacting bilayers. When j is AF, the system is similar to the cuprates[7] described above but the QSF reduces M_s by only 13% because $S = 3/2$. When j is F, there is no QSF reduction of M_s. An important question is how J and j interfere with each other. To study this interesting problem we have calculated the magnetic excitations and QSF for the interacting Quantum Spin dimer problem using a

Heisenberg quantum Hamiltonian.

We investigate the difference in magnon dispersion and QSF between Cr_2XO_6 (X=Mo,W) and Cr_2TeO_6 at zero temperature using a two parameter (J, j) spin 3/2 quantum Heisenberg Hamiltonian. Our calculations use the well known Dyson[15,16] and Maleev[17,18] representation which facilitates the calculations significantly compared to the Holstein-Primakov representation[19]. The paper is organized as follows: we define the Hamiltonian in Section II and discuss the formalism using non-linear spin-wave theory[5,20] along with results for the AF-AF bilayers (Section II A) and F-AF bilayers (Section II B). In Section III we present the results for the magnon dispersion and sublattice magnetization and in Section IV the basic differences between the ground state properties when the inter-bilayer coupling is turned on between the two different types of long range ordered bilayers are discussed. We conclude our paper with a brief conclusion in Section V.

II. FORMALISM

It is well-known that quantum fluctuations play a significant role in the magnetic properties[1,2] and phase diagram of the system at zero temperature.[3–6,20–23] Here we investigate the role of quantum fluctuations on the stability of the Néel state by calculating the magnon spectrum and see how these excitations reduce the sublattice magnetization from its Néel state value. We first express the fluctuations around the classical long range ordered antiferromagnetic ground state in terms of the boson operators using the Dyson-Maleev representation. The quadratic term in boson operators corresponds to the linear spin-wave theory (LSWT), whereas the higher-order terms represent interactions between magnons. We keep terms up to second order in $1/S$. From the renormalized magnon Green's functions and self-energies we calculate the magnon energy dispersion and the normalized sublattice magnetization (NSM) up to and including terms of order $1/S^2$.

A. AF-AF Bilayer

As discussed in Section II there are four chromium atoms in the tetragonal unit cell (shown in Fig. 1). Within each bilayer the spins of Cr1 and Cr3 are coupled antoferromagnetically with the spins of Cr2 and Cr4 respectively through the intra-bilayer NN coupling.

On the other hand, the NN Cr1 and Cr3 spins belonging to different bilayers are coupled antiferromagnetically within the same unit cell whereas Cr2 spin is coupled antiferromagnetically to Cr4 spin in the unit cell below and Cr4 spin is coupled with Cr2 in the unit cell above.

The Hamiltonian of the system with N_z bilayers with antiferromagnetic intra- and inter-bilayer couplings j and J ($j,\ J > 0$) takes the form

$$\begin{aligned} H = j \sum_{n=1}^{N_z} \sum_{\langle i,j \rangle} \Big[\mathbf{S}_{in}^{(1)A} \cdot \mathbf{S}_{jn}^{(2)B} + \mathbf{S}_{in}^{(3)B} \cdot \mathbf{S}_{jn}^{(4)A} \Big] \\ + J \sum_{n=1}^{N_z} \sum_{i} \Big[\mathbf{S}_{in}^{(1)A} \cdot \mathbf{S}_{in}^{(3)B} + \frac{1}{2} \{ \mathbf{S}_{in}^{(2)B} \cdot \mathbf{S}_{in-1}^{(4)A} + \mathbf{S}_{in}^{(4)A} \cdot \mathbf{S}_{in+1}^{(2)B} \} \Big], \end{aligned} \tag{1}$$

where n represents the n-th unit cell index along the z-direction and i, j are nearest-neighbor sites within the same bilayer inside a unit cell. For example, $\mathbf{S}_{in}^{(1)A}$ represents the spin of Cr1 at site i in the n-th unit cell whereas $\mathbf{S}_{jn+1}^{(2)B}$ represents spin of Cr2 in the $(n+1)$-th unit cell. A and B are indices for sublattices A and B. Within the bilayer spins of Cr1, Cr4 are in A sublattice and Cr2, Cr3 are in B sublattice. This spin Hamiltonian is mapped onto an equivalent Hamiltonian of interacting bosons by expressing the spin operators in terms of bosonic creation and annihilation operators $a^\dagger, a$ for "up" sites on sublattice A (and $b^\dagger, b$ for "down" sites on sublattice B) using the Dyson-Maleev representation (dropping the indices i and n for the sake of illustration)[15–18]

$$S_{Ai}^{+} = \sqrt{2S} \Big[a_i - \frac{a_i^\dagger a_i a_i}{(2S)} \Big],\ S_{Ai}^{-} = \sqrt{2S} a_i^\dagger,\ S_{Ai}^{z} = S - a_i^\dagger a_i, \tag{2a}$$

$$S_{Bj}^{+} = \sqrt{2S} \Big[b_j^\dagger - \frac{b_j^\dagger b_j^\dagger b_j}{(2S)} \Big],\ S_{Bj}^{-} = \sqrt{2S} b_j,\ S_{Bj}^{z} = -S + b_j^\dagger b_j. \tag{2b}$$

Substituting Eqs. (2) into Eq. (1) we expand the Hamiltonian perturbatively in powers of $1/S$ as

$$H = H_{-1} + H_0 + H_1 + \cdots, \tag{3}$$

where H_m is of order $1/S^{m-1}$. Note that H_{-1} is just a number representing the classical energy. We do not discuss it further as it is irrelevant for the quantum fluctuations. Hence the $1/S$ expansion will be performed around the unperturbed Hamiltonian H_0 which is the zeroth order Hamiltonian in this sense. Relative to H_0 the terms H_1 and H_2 are first and second order terms respectively which are:

$$
\begin{aligned}
H_{-1} &= -2jNS^2(4+\eta), \qquad &(4a)\\
H_0 &= jS\sum_{n=1}^{N_z}\sum_{\langle i,j\rangle}\Big[a_{in}^{(1)\dagger}a_{in}^{(1)} + a_{in}^{(4)\dagger}a_{in}^{(4)} + b_{jn}^{(2)\dagger}b_{jn}^{(2)} + b_{jn}^{(3)\dagger}b_{jn}^{(3)}\\
&\quad + a_{in}^{(1)}b_{jn}^{(2)} + a_{in}^{(4)}b_{jn}^{(3)} + a_{in}^{(1)\dagger}b_{jn}^{(2)\dagger} + a_{in}^{(4)\dagger}b_{jn}^{(3)\dagger}\Big]\\
&\quad + JS\sum_{n=1}^{N_z}\sum_{i}\Big[a_{in}^{(1)\dagger}a_{in}^{(1)} + b_{in}^{(3)\dagger}b_{in}^{(3)} + a_{in}^{(1)}b_{in}^{(3)} + a_{in}^{(1)\dagger}b_{in}^{(3)\dagger}\\
&\quad + \frac{1}{2}\Big\{a_{in-1}^{(4)\dagger}a_{in-1}^{(4)} + b_{in}^{(2)\dagger}b_{in}^{(2)} + a_{in}^{(4)\dagger}a_{in}^{(4)} + b_{in+1}^{(2)\dagger}b_{in+1}^{(2)}\\
&\quad + a_{in}^{(4)}b_{in+1}^{(2)} + a_{in}^{(4)\dagger}b_{in+1}^{(2)\dagger} + a_{in-1}^{(4)}b_{in}^{(2)} + a_{in-1}^{(4)\dagger}b_{in}^{(2)\dagger}\Big\}\Big], &(4b)\\
H_1 &= -\frac{1}{2}j\sum_{n=1}^{N_z}\sum_{\langle i,j\rangle}\Big[2a_{in}^{(1)\dagger}a_{in}^{(1)}b_{jn}^{(2)\dagger}b_{jn}^{(2)} + 2a_{in}^{(4)\dagger}a_{in}^{(4)}b_{jn}^{(3)\dagger}b_{jn}^{(3)}\\
&\quad + a_{in}^{(1)\dagger}a_{in}^{(1)}a_{in}^{(1)}b_{jn}^{(2)} + a_{in}^{(4)\dagger}a_{in}^{(4)}a_{in}^{(4)}b_{jn}^{(3)} + a_{in}^{(1)\dagger}b_{jn}^{(2)\dagger}b_{jn}^{(2)\dagger}b_{jn}^{(2)} + a_{in}^{(4)\dagger}b_{jn}^{(3)\dagger}b_{jn}^{(3)\dagger}b_{jn}^{(3)}\Big]\\
&\quad - \frac{1}{2}J\sum_{n=1}^{N_z}\sum_{i}\Big[2a_{in}^{(1)\dagger}a_{in}^{(1)}b_{jn}^{(3)\dagger}b_{jn}^{(3)} + a_{in}^{(4)\dagger}a_{in}^{(4)}b_{jn+1}^{(2)\dagger}b_{jn+1}^{(2)} + a_{in-1}^{(4)\dagger}a_{in-1}^{(4)}b_{in}^{(2)\dagger}b_{in}^{(2)}\\
&\quad + \frac{1}{2}\Big\{2a_{in}^{(1)\dagger}a_{in}^{(1)}a_{in}^{(1)}b_{in}^{(3)} + 2a_{in}^{(1)\dagger}b_{in}^{(3)\dagger}b_{in}^{(3)\dagger}b_{in}^{(3)} + a_{in-1}^{(4)\dagger}a_{in-1}^{(4)}a_{in-1}^{(4)}b_{in}^{(2)}\\
&\quad + a_{in}^{(4)\dagger}a_{in}^{(4)}a_{in}^{(4)}b_{in+1}^{(2)} + a_{in}^{(4)\dagger}b_{in+1}^{(2)\dagger}b_{in+1}^{(2)\dagger}b_{in+1}^{(2)} + a_{in-1}^{(4)\dagger}b_{in}^{(2)\dagger}b_{in}^{(2)\dagger}b_{in}^{(2)}\Big\}\Big]. &(4c)
\end{aligned}
$$

In Eq. (4a), the parameter $\eta = J/j$ and $N = N_xN_yN_z$ is the total number of unit cells. Next the real space Hamiltonian is transformed to momentum space using the Fourier transformation for each ℓ-th spin:

$$
a_{in}^{(\ell)} = \frac{1}{\sqrt{N}}\sum_{\mathbf{k}} e^{i\mathbf{k}\cdot\mathbf{R}_{\mathbf{in}}^{(\ell)}}a_{\mathbf{k}}^{(\ell)}, \quad b_{in}^{(\ell)} = \frac{1}{\sqrt{N}}\sum_{\mathbf{k}} e^{-i\mathbf{k}\cdot\mathbf{R}_{\mathbf{in}}^{(\ell)}}b_{-\mathbf{k}}^{(\ell)} \tag{5}
$$

and then we use the following canonical transformations

$$
a_{\mathbf{k}}^{(\ell)} = \exp\Big[-\frac{ik_z}{2}(\frac{c}{2}-\delta)\Big]a_{\mathbf{k}},\ b_{-\mathbf{k}}^{(\ell)} = \exp\Big[-\frac{ik_z}{2}(\frac{c}{2}-\delta)\Big]b_{-\mathbf{k}}, \tag{6}
$$

where δ is the inter-dimer separation (Fig. 1). Finally, we diagonalize the quadratic part H_0 by transforming the operators $a_{\mathbf{k}}$ and $b_{\mathbf{k}}$ to magnon operators $\alpha_{\mathbf{k}}$ and $\beta_{\mathbf{k}}$ using the Bogoliubov (BG) transformations

$$
a_{\mathbf{k}}^{\dagger} = l_{\mathbf{k}}\alpha_{\mathbf{k}}^{\dagger} + m_{\mathbf{k}}\beta_{-\mathbf{k}}, \quad b_{-\mathbf{k}} = m_{\mathbf{k}}\alpha_{\mathbf{k}}^{\dagger} + l_{\mathbf{k}}\beta_{-\mathbf{k}}. \tag{7}
$$

The coefficients $l_{\mathbf{k}}$ and $m_{\mathbf{k}}$ are defined as

$$l_{\mathbf{k}} = \Big[\frac{1+\epsilon_{\mathbf{k}}}{2\epsilon_{\mathbf{k}}}\Big]^{1/2}, \quad m_{\mathbf{k}} = -\mathrm{sgn}(\gamma_{\mathbf{k}})\Big[\frac{1-\epsilon_{\mathbf{k}}}{2\epsilon_{\mathbf{k}}}\Big]^{1/2} \equiv -x_{\mathbf{k}} l_{\mathbf{k}}, \quad x_{\mathbf{k}} = \mathrm{sgn}(\gamma_{\mathbf{k}})\Big[\frac{1-\epsilon_{\mathbf{k}}}{1+\epsilon_{\mathbf{k}}}\Big]^{1/2}, \tag{8}$$

where

$$\gamma_{1\mathbf{k}} = \cos(k_x a/2)\cos(k_y a/2), \quad \gamma_{2\mathbf{k}} = \exp(-ik_z c/2), \quad \gamma_{\mathbf{k}} = \frac{4\gamma_{1\mathbf{k}} + \eta\gamma_{2\mathbf{k}}}{4+\eta}, \tag{9a}$$

$$\epsilon_{\mathbf{k}} = (1 - |\gamma_{\mathbf{k}}|^2)^{1/2}. \tag{9b}$$

The resulting expressions in terms of magnon operators are:

$$H_{-1} = -2jNS^2(4+\eta), \tag{10a}$$

$$H_0 = 2jS(4+\eta)\sum_{\mathbf{k}}\Big[\epsilon_{\mathbf{k}}\left(\alpha^\dagger_{\mathbf{k}}\alpha_{\mathbf{k}} + \beta^\dagger_{-\mathbf{k}}\beta_{-\mathbf{k}}\right) + (\epsilon_{\mathbf{k}} - 1)\Big], \tag{10b}$$

$$H_1 = \frac{2jS(4+\eta)}{(2S)}\Big\{\sum_{\mathbf{k}} A_{\mathbf{k}}\left(\alpha^\dagger_{\mathbf{k}}\alpha_{\mathbf{k}} + \beta^\dagger_{-\mathbf{k}}\beta_{-\mathbf{k}}\right) \tag{10c}$$

$$\begin{aligned}
&-\frac{1}{N}\sum_{1234}\delta_{\mathbf{G}}(1+2-3-4)(2l_1l_2l_3l_4)\Big[V^{(1)}_{12;34}\alpha^\dagger_1\alpha^\dagger_2\alpha_3\alpha_4 + 2V^{(2)}_{12;34}\alpha^\dagger_1\beta_{-2}\alpha_3\alpha_4 \\
&+ 2V^{(3)}_{12;34}\alpha^\dagger_1\alpha^\dagger_2\beta^\dagger_{-3}\alpha_4 + 4V^{(4)}_{12;34}\alpha^\dagger_1\alpha_3\beta^\dagger_{-4}\beta_{-2} + 2V^{(5)}_{12;34}\beta^\dagger_{-4}\alpha_3\beta_{-2}\beta_{-1} + 2V^{(6)}_{12;34}\beta^\dagger_{-4}\beta^\dagger_{-3}\alpha^\dagger_2\beta_{-1} \\
&+ V^{(7)}_{12;34}\alpha^\dagger_1\alpha^\dagger_2\beta^\dagger_{-3}\beta^\dagger_{-4} + V^{(8)}_{12;34}\beta_{-1}\beta_{-2}\alpha_3\alpha_4 + V^{(9)}_{12;34}\beta^\dagger_{-4}\beta^\dagger_{-3}\beta_{-2}\beta_{-1}\Big]\Big\}.
\end{aligned} \tag{10d}$$

The coefficient $A_{\mathbf{k}}$ is given by

$$A_{\mathbf{k}} = \Big[\frac{1}{N}\sum_{\mathbf{p}}\frac{\epsilon_{\mathbf{p}} + |\gamma_{\mathbf{p}}|^2 - 1}{\epsilon_{\mathbf{p}}}\Big]\epsilon_{\mathbf{k}}. \tag{11}$$

In Eq. (10d) momenta $\mathbf{k}_1, \mathbf{k}_2, \mathbf{k}_3, \mathbf{k}_4$ are abbreviated as 1, 2, 3, and 4. The first term (Eq. (10a)) is the classical Néel energy, the second term (Eq. 10b) represents the excitation energy of the magnons within LSWT of $O(S^0)$ and the leading order quantum zero-point energy, the term proportional to $(\epsilon_{\mathbf{k}} - 1)$, and the third term (Eq. (10d)) comprises $1/S$ contribution to the Hamiltonian. The first term in Eq. (10d) is obtained by normal ordering the products of four boson operators with respect to creation and annihilation in the magnon operators, i.e. magnon creation operators appear always to the left of magnon annihilation operators. We have omitted the corrections to the ground state energy in Eq. (10d) as they are not relevant to our calculations for the energy dispersion and magnetization.

The quasiparticle energy $\tilde{E}^{\mathrm{AF}}_{\mathbf{k},\alpha\alpha}$ for the α-magnon excitations measured in units of $2jS(4+\eta)$ up to second order in $1/S$ is given as

$$\tilde{E}^{\mathrm{AF}}_{\mathbf{k},\alpha\alpha} = 2jS(4+\eta)\Big[\epsilon_{\mathbf{k}} + \frac{1}{(2S)}A_{\mathbf{k}} + \frac{1}{(2S)^2}\Sigma^{(2)}_{\alpha\alpha}(\mathbf{k}, \epsilon_{\mathbf{k}})\Big]. \tag{12}$$

Expressions for the magnon Green's functions and self-energies are given in Appendix A. The dynamic contributions to the second order self-energies $\Sigma^{(2)}$ are second order in the vertex factors $V^{(j)}$. These are the contributions which are missed by self-consistent spin-wave theory. Explicit forms of the vertex factors required for our calculations are given in Appendix B 1.

Analytical expressions for the energy dispersion can be derived from the LSWT expression using Eq. (10b) for different regions in $\mathbf{k}$ space. They are:

$$E^{I}(k_x,0,0) = 8jS\sin\left(\frac{k_xa}{4}\right)\sqrt{\eta+4\cos^2\left(\frac{k_xa}{4}\right)},\quad (0\le k_x\le\frac{\pi}{a}) \tag{13a}$$

$$E^{II}(\frac{\pi}{a},k_y,0) = 4\sqrt{2}jS\sqrt{\eta+2},\quad (0\le k_y\le\frac{\pi}{a}) \tag{13b}$$

$$E^{III}(\frac{\pi}{a},\frac{\pi}{a},k_z) = 4\sqrt{2}jS\sqrt{\eta+2},\quad (0\le k_z\le\frac{\pi}{c}) \tag{13c}$$

$$E^{IV}(k_x,k_y,\frac{\pi}{c}) = 4\sqrt{2}jS\sqrt{\eta+2\Big[1-\cos^2(\frac{k_xa}{2})\cos^2(\frac{k_ya}{2})\Big]},\quad (0\le k_x,k_y\le\frac{\pi}{a}) \tag{13d}$$

$$E^{V}(0,0,k_z) = 8jS\sqrt{\eta}\sin\left(\frac{k_zc}{4}\right).\quad (0\le k_z\le\frac{\pi}{c}) \tag{13e}$$

The expressions for the sublattice magnetization are shown in Eq. (A7). In contrast to the quasi-particle energy, there is no first-order $1/S$ correction to the magnetization ($M_1 = 0$ for the AF-AF bilayer) as there are no off-diagonal $B_{\mathbf{k}}$ terms in Eq. (10d).

B. F-AF Bilayer

In this case the NN intra-bilayer couplings j between Cr1 with Cr2 and Cr3 with Cr4 are ferromagnetic whereas the inter-bilayer couplings J are antiferromagnetic between Cr1 with Cr3 within the same inter-bilayer and Cr2 spin with Cr4 spin between the adjacent up or down unit cells.

$$\begin{aligned}H = &-j\sum_{n=1}^{N_z}\sum_{\langle i,j\rangle}\Big[\mathbf{S}^{(1)A}_{in}\cdot\mathbf{S}^{(2)A}_{jn}+\mathbf{S}^{(3)B}_{in}\cdot\mathbf{S}^{(4)B}_{jn}\Big]\\ &+J\sum_{n=1}^{N_z}\sum_{i}\Big[\mathbf{S}^{(1)A}_{in}\cdot\mathbf{S}^{(3)B}_{in}+\frac{1}{2}\{\mathbf{S}^{(2)A}_{in}\cdot\mathbf{S}^{(4)B}_{in-1}+\mathbf{S}^{(4)B}_{in}\cdot\mathbf{S}^{(2)A}_{in+1}\}\Big].\end{aligned} \tag{14}$$

Here within the tetragonal unit cell Cr1, Cr2 are in A sublattice and Cr3, Cr4 are in B sublattice. We then map the spin Hamiltonian onto an equivalent Hamiltonian of interacting bosons using the DM transformation to obtain:

$$
\begin{aligned}
H_{-1} &= -2jNS^2(4+\eta), &\text{(15a)}\\
H_0 &= jS\sum_{n=1}^{N_z}\sum_{\langle i,j\rangle}\Big[a_{in}^{(1)\dagger}a_{in}^{(1)} + a_{in}^{(2)\dagger}a_{in}^{(2)} + b_{jn}^{(3)\dagger}b_{jn}^{(3)} + b_{jn}^{(4)\dagger}b_{jn}^{(4)}\\
&\quad - a_{in}^{(1)}a_{jn}^{(2)\dagger} - a_{in}^{(1)\dagger}a_{jn}^{(2)} - b_{in}^{(3)\dagger}b_{jn}^{(4)} - b_{in}^{(3)}b_{jn}^{(4)\dagger}\Big]\\
&\quad + JS\sum_{n=1}^{N_z}\sum_{i}\Big[a_{in}^{(1)\dagger}a_{in}^{(1)} + b_{in}^{(3)\dagger}b_{in}^{(3)} + a_{in}^{(1)}b_{in}^{(3)} + a_{in}^{(1)\dagger}b_{in}^{(3)\dagger}\\
&\quad + \frac{1}{2}\Big\{a_{in}^{(2)\dagger}a_{in}^{(2)} + a_{in+1}^{(2)\dagger}a_{in+1}^{(2)} + b_{in}^{(4)\dagger}b_{in}^{(4)} + b_{in-1}^{(4)\dagger}b_{in-1}^{(4)}\\
&\quad + a_{in}^{(2)}b_{in-1}^{(4)} + a_{in}^{(2)\dagger}b_{in-1}^{(4)\dagger} + a_{in+1}^{(2)}b_{in}^{(4)} + a_{in+1}^{(2)\dagger}b_{in}^{(4)\dagger}\Big\}\Big], &\text{(15b)}\\
H_1 &= -\frac{1}{2}j\sum_{n=1}^{N_z}\sum_{\langle i,j\rangle}\Big[2a_{in}^{(1)\dagger}a_{in}^{(1)}a_{jn}^{(2)\dagger}a_{jn}^{(2)} + 2b_{in}^{(3)\dagger}b_{in}^{(3)}b_{jn}^{(4)\dagger}b_{jn}^{(4)}\\
&\quad - a_{in}^{(1)\dagger}a_{in}^{(1)}a_{in}^{(1)}a_{jn}^{(2)\dagger} - a_{in}^{(1)\dagger}a_{jn}^{(2)\dagger}a_{jn}^{(2)}a_{jn}^{(2)} - b_{in}^{(3)\dagger}b_{in}^{(3)\dagger}b_{in}^{(3)}b_{jn}^{(4)} - b_{in}^{(3)}b_{jn}^{(4)\dagger}b_{jn}^{(4)\dagger}b_{jn}^{(4)}\Big]\\
&\quad - \frac{1}{2}J\sum_{n=1}^{N_z}\sum_{i}\Big[2a_{in}^{(1)\dagger}a_{in}^{(1)}b_{in}^{(3)\dagger}b_{in}^{(3)} + a_{in}^{(2)\dagger}a_{in}^{(2)}b_{in-1}^{(4)\dagger}b_{in-1}^{(4)} + a_{in+1}^{(2)\dagger}a_{in+1}^{(2)}b_{in}^{(4)\dagger}b_{in}^{(4)}\\
&\quad + \frac{1}{2}\Big\{2a_{in}^{(1)\dagger}a_{in}^{(1)}a_{in}^{(1)}b_{in}^{(3)} + 2a_{in}^{(1)\dagger}b_{in}^{(3)\dagger}b_{in}^{(3)\dagger}b_{in}^{(3)} + a_{in}^{(2)\dagger}a_{in}^{(2)}a_{in}^{(2)}b_{in-1}^{(4)}\\
&\quad + a_{in}^{(2)\dagger}b_{in-1}^{(4)\dagger}b_{in-1}^{(4)\dagger}b_{in-1}^{(4)} + a_{in+1}^{(2)\dagger}b_{in}^{(4)\dagger}b_{in}^{(4)\dagger}b_{in}^{(4)} + a_{in+1}^{(2)\dagger}a_{in+1}^{(2)}a_{in+1}^{(2)\dagger}b_{in}^{(4)}\Big\}\Big]. &\text{(15c)}
\end{aligned}
$$

After Fourier transformation into the **k** space and using the canonical transformations

$$
\begin{aligned}
a_{\mathbf{k}}^{((1)} &= \exp\Big[-\frac{ik_z}{2}(\frac{c}{2}-\delta)\Big]a_{\mathbf{k}},\ a_{\mathbf{k}}^{((2)} = \exp\Big[\frac{ik_z}{2}(\frac{c}{2}-\delta)\Big]a_{\mathbf{k}}, &\text{(16a)}\\
b_{-\mathbf{k}}^{(3)} &= \exp\Big[-\frac{ik_z}{2}(\frac{c}{2}-\delta)\Big]b_{-\mathbf{k}},\ b_{-\mathbf{k}}^{(4)} = \exp\Big[\frac{ik_z}{2}(\frac{c}{2}-\delta)\Big]b_{-\mathbf{k}}, &\text{(16b)}
\end{aligned}
$$

the Hamiltonian in Eq. (15) becomes:

$$
\begin{aligned}
H_{-1} &= -2jNS^2(4+\eta), &\text{(17a)}\\
H_0 &= 2jS\sum_{\mathbf{k}}\Big[\kappa_{\mathbf{k}}\epsilon_{\mathbf{k}}\left(\alpha_{\mathbf{k}}^\dagger\alpha_{\mathbf{k}} + \beta_{-\mathbf{k}}^\dagger\beta_{-\mathbf{k}}\right) + \kappa_{\mathbf{k}}(\epsilon_{\mathbf{k}}-1)\Big], &\text{(17b)}\\
H_1 &= \frac{2jS}{(2S)}\sum_{\mathbf{k}}\Big[A_{\mathbf{k}}\left(\alpha_{\mathbf{k}}^\dagger\alpha_{\mathbf{k}} + \beta_{-\mathbf{k}}^\dagger\beta_{-\mathbf{k}}\right) + B_{\mathbf{k}}\left(\alpha_{\mathbf{k}}^\dagger\beta_{-\mathbf{k}}^\dagger + \alpha_{\mathbf{k}}\beta_{-\mathbf{k}}\right) &\text{(17c)}\\
&\quad - \frac{1}{N}\sum_{1234}\delta_{\mathbf{G}}(1+2-3-4)(2l_1l_2l_3l_4)\Big[V_{12;34}^{(1)}\alpha_1^\dagger\alpha_2^\dagger\alpha_3\alpha_4 + 2V_{12;34}^{(2)}\alpha_1^\dagger\beta_{-2}\alpha_3\alpha_4\\
&\quad + 2V_{12;34}^{(3)}\alpha_1^\dagger\alpha_2^\dagger\beta_{-3}^\dagger\alpha_4 + 4V_{12;34}^{(4)}\alpha_1^\dagger\alpha_3\beta_{-4}^\dagger\beta_{-2} + 2V_{12;34}^{(5)}\beta_{-4}^\dagger\alpha_3\beta_{-2}\beta_{-1} + 2V_{12;34}^{(6)}\beta_{-4}^\dagger\beta_{-3}^\dagger\alpha_2^\dagger\beta_{-1}\\
&\quad + V_{12;34}^{(7)}\alpha_1^\dagger\alpha_2^\dagger\beta_{-3}^\dagger\beta_{-4}^\dagger + V_{12;34}^{(8)}\beta_{-1}\beta_{-2}\alpha_3\alpha_4 + V_{12;34}^{(9)}\beta_{-4}^\dagger\beta_{-3}^\dagger\beta_{-2}\beta_{-1}\Big]\Big]. &\text{(17d)}
\end{aligned}
$$

where

$$\gamma_{1\mathbf{k}} = \cos(k_x a/2)\cos(k_y a/2), \quad \gamma_{2\mathbf{k}} = \cos(k_z c/2), \tag{18a}$$

$$\kappa_{\mathbf{k}} = 4(1-\gamma_{1\mathbf{k}}) + \eta, \quad \gamma_{\mathbf{k}} = \frac{\eta\gamma_{2\mathbf{k}}}{\kappa_{\mathbf{k}}}, \tag{18b}$$

$$\epsilon_{\mathbf{k}} = (1-|\gamma_{\mathbf{k}}|^2)^{1/2}, \quad E_{\mathbf{k}} = \kappa_{\mathbf{k}}\epsilon_{\mathbf{k}}, \tag{18c}$$

$$A_1 = \frac{2}{N}\sum_{\mathbf{k}} \frac{1-\epsilon_{\mathbf{k}}-\gamma_{1\mathbf{k}}}{\epsilon_{\mathbf{k}}}, \quad A_2 = \frac{1}{N}\sum_{\mathbf{k}} \frac{1-\epsilon_{\mathbf{k}}-\gamma_{\mathbf{k}}\gamma_{2\mathbf{k}}}{2\epsilon_{\mathbf{k}}}, \tag{18d}$$

$$A_{\mathbf{k}} = -\frac{2}{\epsilon_{\mathbf{k}}}[A_1(1-\gamma_{1\mathbf{k}}) + \eta A_2(1-\gamma_{\mathbf{k}}\gamma_{2\mathbf{k}})], \tag{18e}$$

$$B_{\mathbf{k}} = \frac{2}{\epsilon_{\mathbf{k}}}[A_1\gamma_{\mathbf{k}}(1-\gamma_{1\mathbf{k}}) - \eta A_2(\gamma_{2\mathbf{k}}-\gamma_{\mathbf{k}})]. \tag{18f}$$

Explicit forms of the vertex factors $V^{i=2,3,5,7,8}_{1234}$ are given in Appendix B 2. Once again, we have omitted the corrections to the ground state energy of $O(S^0)$ in Eq. (17d) as they are not relevant to our calculations for magnon dispersion and sublattice magnetization.

The quasiparticle energy $\tilde{E}^{\mathrm{F}}_{\mathbf{k},\alpha\alpha}$ for α-magnon excitations, measured in units of $2jS$ up to second order in $1/S$ is given as

$$\tilde{E}^{\mathrm{F}}_{\mathbf{k},\alpha\alpha} = 2jS\Big[E_{\mathbf{k}} + \frac{1}{(2S)}A_{\mathbf{k}} + \frac{1}{(2S)^2}\Big\{\Sigma^{(2)}_{\alpha\alpha}(\mathbf{k},E_{\mathbf{k}}) - \frac{B^2_{\mathbf{k}}}{2E_{\mathbf{k}}}\Big\}\Big]. \tag{19}$$

Similar to the AF-AF bilayer, analytical expressions for the energy dispersion can be derived from the LSWT expression using Eq. (18c) for different regions. They are:

$$E^{I}(k_x,0,0) = 8jS\sin\left(\frac{k_x a}{4}\right)\sqrt{\eta + 4\sin^2\left(\frac{k_x a}{4}\right)}, \;\; (0 \le k_x \le \frac{\pi}{a}) \tag{20a}$$

$$E^{II}(\frac{\pi}{a},k_y,0) = 4\sqrt{2}jS\sqrt{\eta+2}, \;\; (0 \le k_y \le \frac{\pi}{a}) \tag{20b}$$

$$E^{III}(\frac{\pi}{a},\frac{\pi}{a},k_z) = 8jS\sqrt{1 + \frac{\eta}{2} + \frac{\eta^2}{16}\sin^2\left(\frac{k_z c}{2}\right)}, \;\; (0 \le k_z \le \frac{\pi}{c}) \tag{20c}$$

$$E^{IV}(k_x,k_y,\frac{\pi}{c}) = 2jS\Big[\eta + 4\Big\{1 - \cos(\frac{k_x a}{2})\cos(\frac{k_y a}{2})\Big\}\Big], \;\; (0 \le k_x, k_y \le \frac{\pi}{a}) \tag{20d}$$

$$E^{V}(0,0,k_z) = 2jS\eta\sin\left(\frac{k_z c}{2}\right). \;\; (0 \le k_z \le \frac{\pi}{c}) \tag{20e}$$

For the F-AF bilayer, the sublattice magnetization in Eq. (A7) has both first-order $1/S$ and second-order $1/S^2$ corrections.

III. RESULTS: ENERGY DISPERSION AND MAGNETIZATION

A. Energy Dispersion

We obtain the spin-wave energy dispersions for AF-AF and F-AF bilayers for $S = 3/2$ as a function of momenta (k_x, k_y, k_z) for three different values of $\eta = J/j$ by evaluating Eqs. (12) and (19) in the first BZ. For the numerical summation we divide the first BZ in a mesh of N_L^3 points with $N_L = 24$. Then the contributions from N_L^3 points of $\mathbf{p}$ and $\mathbf{q}$ in the first BZ are summed up to evaluate the third terms in Eqs. (12) and (19). In the Dyson-Maleev formalism no cancellation of divergences occurs so that the convergence of the numerical results for $N_L \to \infty$ is very good.[24] This is a crucial advantage over the use of the Holstein-Primakov representation. Our results for dispersion with $N_L = 24$ are accurate at least up to four significant digits.

In Fig. 2 we show the energy-dispersions (for α-magnon excitations) calculated with LSWT (dashed lines), with $1/S$ corrections (dot-dashed lines in blue), and with $1/S^2$ corrections (solid lines) for the AF-AF and F-AF bilayers for $\eta = J/j = 5.0$. In both cases (a) and (b) $1/S$ corrections are significantly large, but $1/S^2$ corrections are less than 0.5% compared to the results with $1/S$ corrections. It is interesting to point out that for the two-dimensional $S = 1/2$ square lattice antiferromagnet with only NN AF interactions the dispersion at $\mathbf{k} = (\pi, 0)$ and at $\mathbf{k} = (\pi/2, \pi/2)$ takes precisely the same value in linear spin-wave theory and with first-order $1/S$ corrections. However, in second order $1/S^2$, a small dip appears which is about 1.4%. This number improves to 3.2% upon going to the third order $1/S^3$.[25] Details can be found in Ref. (5) and (22). For our case the spin S being large, the higher-order corrections are significantly smaller and can be neglected. For the F-AF bilayer in Fig. 2(b) $1/S^2$ corrections are only noticeable between the region $(\pi/a, 0, 0) - (\pi/a, \pi/a, 0)$ where the dispersion is about 1% less than the dispersion calculated with only $1/S$ corrections.

The spin-wave energy dispersions (for both LSWT and with $1/S^2$ corrections) are shown in Fig. 3 for three different values of eta. For $\eta = 0$ $(J = 0)$ the bilayers are decoupled and we essentially have a decoupled $2D$ system. In this case we reproduce the existing results as shown in Fig. 3 – there is no energy dispersion between $(0, 0, \pi/c) - (0, 0, 0)$. Note that for Fig. 3(a) the dispersion is shown in units of $2jS(4 + \eta)$. So to compare the results with

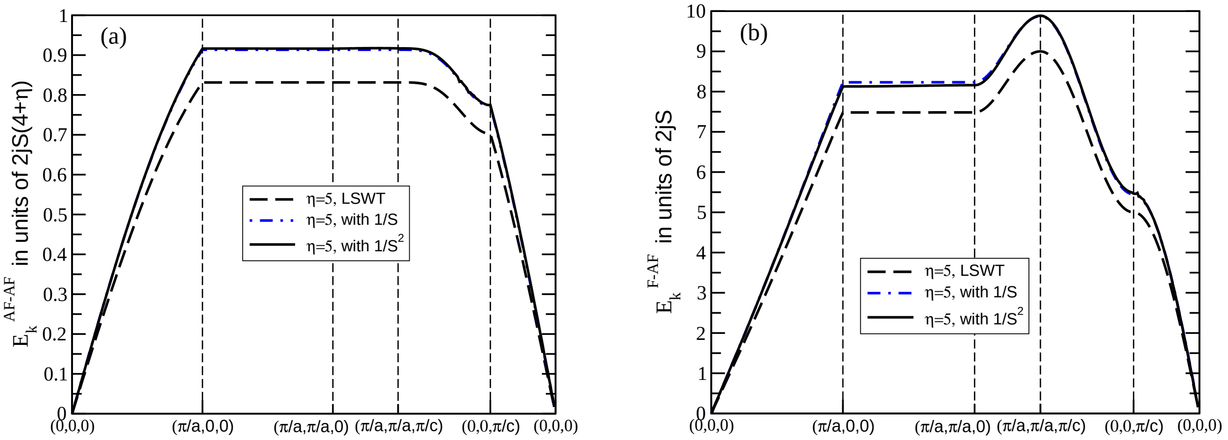

FIG. 2. (Color online) Spin-wave energy dispersion for the α-magnon excitations $E_{\mathbf{k},\alpha\alpha}$ for the (a) AF-AF and (b) F-AF bilayers are plotted for $\eta = 5.0$. Results from LSWT (dashed lines), with $1/S$ correction (dot-dashed in blue), and with $1/S^2$ corrections (solid lines) are shown. For the AF-AF bilayer $1/S$ corrections harden the magnon dispersion and are significant ($\sim 10\%$) of LSWT results but $1/S^2$ corrections soften the spectrum but are hardly noticeable from the $1/S$ results ($< 0.5\%$ for most of the region except between $(\pi/a, 0, 0) - (\pi/a, \pi/a, 0)$. For F-AF bilayer, $1/S$ corrections harden the spectrum (by $\sim 10\%$) from the LSWT results whereas the $1/S^2$ corrections lower the dispersion by about 1%.

the analytical LSWT results for five regions given in Eqs. (13a) -(13e) we have to multiply our numerical data by the factor $2jS(4+\eta)$. On the other hand, the dispersion for the F-AF bilayer displayed in Fig. 3(b) is in units of $2jS$. A peak at $(\pi/a, \pi/a, \pi/c)$ becomes more pronounced with increasing values of η in this case. Similar to the AF -AF bilayer, the energy dispersions for the regions I-V can be checked against the analytical results obtained from LSWT as given in Eqs. (20a) -(20e).

B. Sublattice Magnetization

We calculate the normalized sublattice magnetization M_s/M_0 from Eq. (A7) by numerically evaluating Eqs. (A8a)–(A8c) as a function of η. Especially to obtain the second order corrections M_2 we sum up the values of $N_L^3/8$ points of $\mathbf{k}$ in one octant of the first BZ and N_L^3 points of $\mathbf{p}$ and $\mathbf{q}$ in the first BZ, with $N_L = 14$ sites along one axis. The calculations are correct up to four significant digits. Fig. 4 shows the magnetizations (both LSWT and with

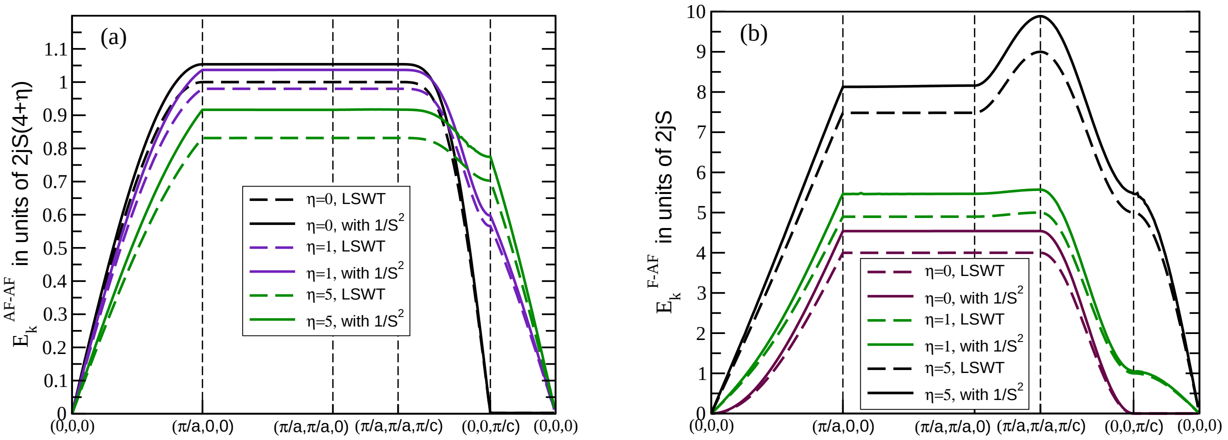

FIG. 3. (Color online) Spin-wave energy dispersion (for α-magnon excitations) $E_{\mathbf{k},\alpha\alpha}$ for the (a) AF-AF and (b) F-AF bilayers are plotted for different values of $\eta = J/j$. Results from LSWT (dashed lines) and with $1/S^2$ corrections (solid lines) are both shown for $\eta = 0,\ 1.0,\ 5.0$. $1/S$ corrections are significantly larger than LSWT results. However, $1/S^2$ corrections are not that significant compared to the results with $1/S$ corrections. For $\eta = 0$, the bilayers are decoupled and we reproduce the existing results for $2D$ Heisenberg antiferromagnet. For Fig. 3(b) a peak at $(\pi/a, \pi/a, \pi/c)$ becomes more pronounced with increasing values of η. For our plots we have chosen $c/a = 2.0$.

$1/S^2$ corrections) for AF-AF and F-AF bilayers as a function of $\eta = J/j$. For Fig. 4(a) there are no first-order $1/S$ corrections to the magnetization (as off-diagonal $B_{\mathbf{k}}$ terms are not present in the quadratic part of Eq.(10d)). Interlayer coupling initially enhances the magnetization up to $\eta = 0.66$ (from $M_s/M_0 = 1.3030$ at $\eta = 0$ to 1.3515 at $\eta = 0.66$) and then with increase in spin-fluctuations magnetization decreases with increase in η. $1/S^2$ terms in the Hamiltonian provide significant corrections to the LSWT results with increase in η as the spin-fluctuations increase. Note that for $\eta = 0$ spin-fluctuations are strong enough to reduce the scaled sublattice magnetization to 1.3030 from the classical value of 1.5 - similar to spin 1/2 $2D$ antiferromagnet on a square lattice where the sublattice magnetization reduces from 0.5 to 0.3067.[5,20]

For Fig. 4(b) as there is no antiferromagnetic inter-bilayer coupling for $\eta = 0$ the bilayers are again decoupled and each bilayer is ferromagnetic. As a result there are no spin fluctuations. With increase in η inter-bilayer AF coupling J introduces spin fluctuation corrections to magnetization which decreases monotonically. $1/S$ terms in the Hamiltonian provide significant corrections to the LSWT results with increase in η. Relative to $1/S$ corrections, $1/S^2$ corrections in this case are insignificant.

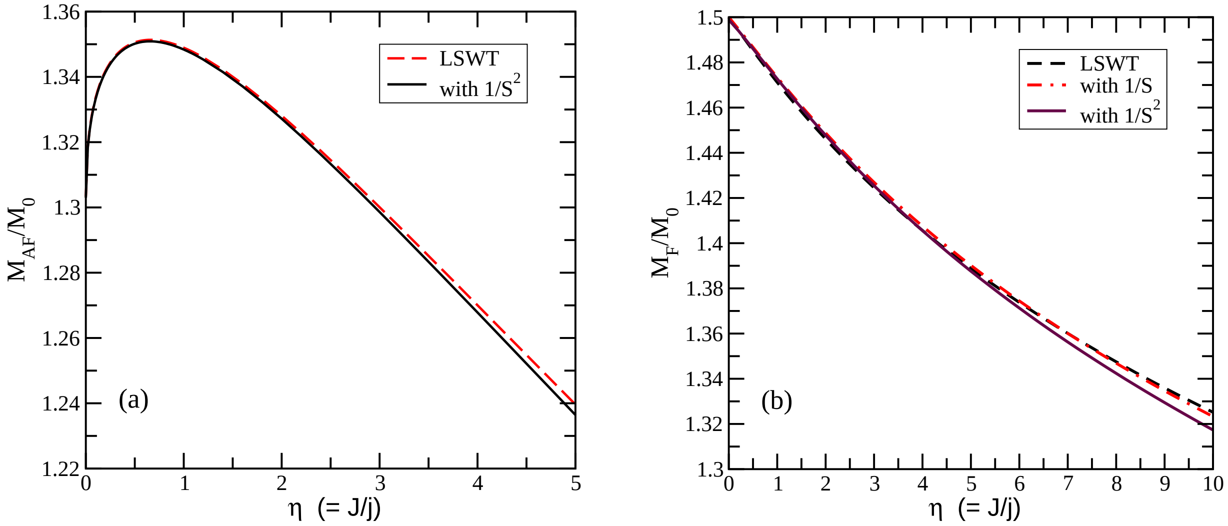

FIG. 4. (Color online) Normalized sublattice magnetization M_s/M_0 for (a) AF-AF and (b) F-AF bilayers as a function of $\eta = J/j$ obtained from LSWT (dashed lines), with $1/S$ (dot-dashed), and with $1/S^2$ corrections (solid lines). For Fig. 4(a) there are no first-order $1/S$ corrections to the magnetization. Magnetization initially increases (spin-fluctuations decreases) up to $\eta \approx 0.66$ and then decreases monotonically as spin-fluctuations increase with η. $1/S^2$ terms in the Hamiltonian provide significant corrections to the LSWT results with increase in η as the spin-fluctuations increase. In Fig. 4(b) when $\eta = 0$ there are no spin fluctuations as the $2D$ system is ferromagnetic (see text). With increase in η, the magnetization monotonically decreases. $1/S$ terms in the Hamiltonian provide significant corrections to the LSWT results with increase in η.

IV. COMPARISON BETWEEN AF-AF AND F-AF BILAYERS

We would like to discuss briefly the basic differences between the ground state properties of two different long range ordered bilayer states when the inter-bilayer coupling is turned on. When $J = 0$ ($\eta = 0$) the bilayers are decoupled and the spin-wave dispersion is quadratic (linear) function of wave vector $\mathbf{k}$ for the F (AF) bilayers, and reduction of the normalized sublattice magnetization M_s/M_0 is 0 ($\sim$13%). When the antiferromagnetic inter-bilayer coupling J ($\eta > 0$) is turned on, the changes in magnon dispersion and renormalization of the sublattice magnetization are dramatically different between the two cases. For the F case magnons harden and the quadratic dispersion along the xy-plane becomes linear for small $\mathbf{k}$ and for large η the spectrum is essentially linear. A large peak develops around $(\pi/a, \pi/a, \pi/c)$ as the value of η increases. In contrast for the AF bilayer where the magnon dispersion is already linear in the basal plane the introduction of AF inter-bilayer coupling does not do much. In fact it softens the magnon spectrum. The effect of non-zero η on M_s/M_0 is simple in the F case, M_s/M_0 decreases monotonically with η, linearly for values of $\eta \approx 2$. For the AF case inter-bilayer coupling first increases M_s/M_0, as intra and inter-bilayer AF couplings compete with each other. When the inter-bilayer coupling becomes large the sublattice magnetization starts to decrease dramatically mimicking the weakly interacting quantum dimer limit. As an example, for the same value of $\eta(=5)$ the values of normalized magnetization M_s/M_0 for the F(AF) case with $1/S^2$ corrections are 1.388 (1.236).

V. CONCLUSIONS

In this work we have investigated the interplay of inter-bilayer and intra-bilayer couplings on magnon dispersion and sublattice magnetization of system with $S = 3/2$. In particular, we studied higher-order quantum effects in a systematic perturbative spin-wave expansion in the inverse spin S. We have calculated the spin-wave energy and the magnetization up to and including the second-order corrections. They contribute significantly to the shape of the magnon spectrum and renormalization of the sublattice magnetization, especially as the ratio of interlayer and intralayer coupling increases.

VI. ACKNOWLEDGMENT

We acknowledge the use of HPC cluster at GVSU, supported by the National Science Foundation Grant No. CNS-1228291 that have contributed to the research results reported within this paper. SDM would like to thank Dr. Xianglin Ke for stimulating discussions.

Appendix A: Green's functions, Self-energies, and Magnetization

The time-ordered magnon Green's functions are defined as

$$G_{\alpha\alpha}(\mathbf{k},t) = -i\langle T(\alpha_{\mathbf{k}}(t)\alpha^{\dagger}_{\mathbf{k}}(0))\rangle, \quad G_{\beta\beta}(\mathbf{k},t) = -i\langle T(\beta^{\dagger}_{-\mathbf{k}}(t)\beta_{-\mathbf{k}}(0))\rangle, \tag{A1a}$$

$$G_{\alpha\beta}(\mathbf{k},t) = -i\langle T(\alpha_{\mathbf{k}}(t)\beta_{-\mathbf{k}}(0))\rangle, \quad G_{\beta\alpha}(\mathbf{k},t) = -i\langle T(\beta^{\dagger}_{-\mathbf{k}}(t)\alpha^{\dagger}_{\mathbf{k}}(0))\rangle, \tag{A1b}$$

Considering H_0 as the unperturbed Hamiltonian the Fourier transformed unperturbed propagators are

$$G^0_{\alpha\alpha}(\mathbf{k},\omega) = \frac{1}{\omega - E_k + i\delta}, \quad G^0_{\beta\beta}(\mathbf{k},\omega) = \frac{1}{-\omega - E_k + i\delta}, \tag{A2a}$$

$$G^0_{\alpha\beta}(\mathbf{k},\omega) = G^0_{\beta\alpha}(\mathbf{k},\omega) = 0, \tag{A2b}$$

with $\delta \to 0+$. The spin-wave energy $E_{\mathbf{k}} = \kappa_{\mathbf{k}}\epsilon_{\mathbf{k}}$ is measured in units of $2JS(4+\eta)$ for the AF-AF bilayer and $2JS$ for the F-AF bilayer. The graphical representations of the Green functions are shown in Fig. 5(a).

The full propagators $G_{ij}(\mathbf{k},\omega)$ satisfy the matrix Dyson equation

$$G_{ij}(\mathbf{k},\omega) = G^0_{ij}(\mathbf{k},\omega) + \sum_{mn} G^0_{im}(\mathbf{k},\omega)\Sigma_{mn}(\mathbf{k},\omega)G_{nj}(\mathbf{k},\omega), \tag{A3}$$

where the self-energy $\Sigma_{ij}(\mathbf{k})$ can be expressed in powers of $1/(2S)$ as

$$\Sigma_{ij}(\mathbf{k},\omega) = \frac{1}{(2S)}\Sigma^{(1)}_{ij}(\mathbf{k},\omega) + \frac{1}{(2S)^2}\Sigma^{(2)}_{ij}(\mathbf{k},\omega) + \ldots. \tag{A4}$$

The first-order self-energy terms read

$$\Sigma^{(1)}_{\alpha\alpha}(\mathbf{k},\omega) = \Sigma^{(1)}_{\beta\beta}(\mathbf{k},\omega) = A_{\mathbf{k}}, \tag{A5a}$$

$$\Sigma^{(1)}_{\alpha\beta}(\mathbf{k},\omega) = \Sigma^{(1)}_{\beta\alpha}(\mathbf{k},\omega) = B_{\mathbf{k}}. \tag{A5b}$$

The second-order self-energy terms originate from the Feynman diagrams in Figs. 5(b),

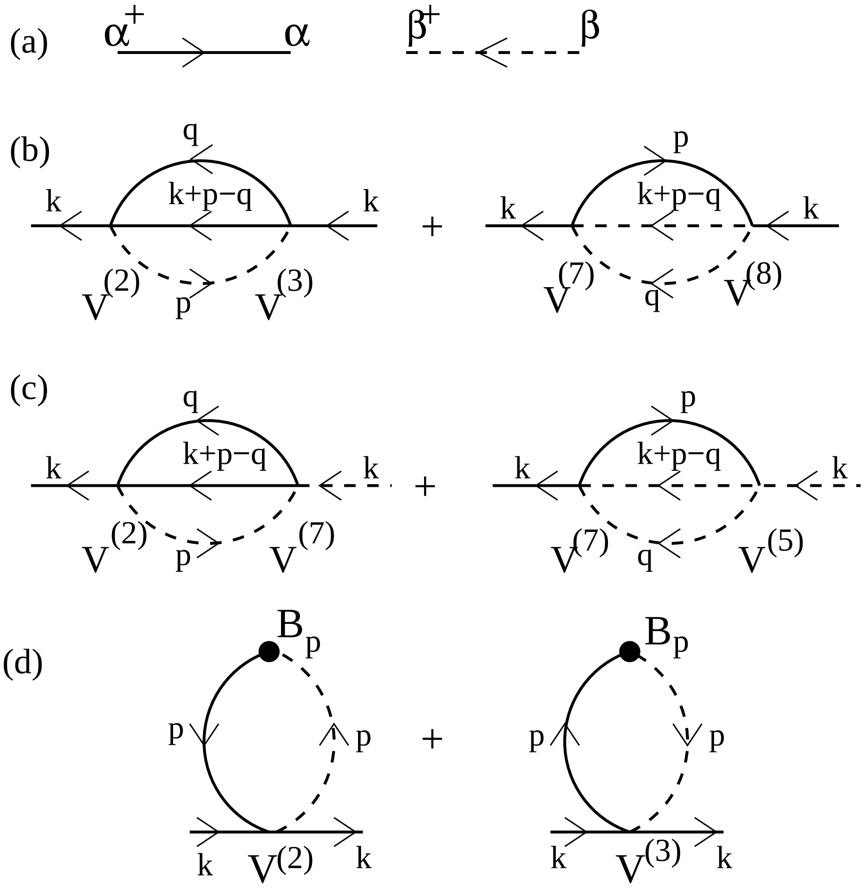

FIG. 5. (a) The solid and the dashed lines correspond to the α and β propagators. Second-order diagrams for the self-energies $\Sigma^{(2)}_{\alpha\alpha}(\mathbf{k},\omega)$ and $\Sigma^{(2)}_{\alpha\beta}(\mathbf{k},\omega)$ are shown in (b) and (c). The diagrams in (d) contribute only to $\Sigma^{(2)}_{\alpha\alpha}(\mathbf{k},\omega)$. $V^{(2)}, V^{(3)}, V^{(5)}, V^{(7)}, V^{(8)}$ are the vertex factors (see main text). Note that at each vertex two arrows enter the vertex and two leave it which reflects the conservation of the total S_z component.

(c), and (d). The complete expressions read

$$\Sigma^{(2)}_{\alpha\alpha}(\mathbf{k},\omega) = \Sigma^{(2)}_{\beta\beta}(\mathbf{k},\omega) = \Big(\frac{1}{N}\Big)\sum_{\mathbf{p}} 2(2\ell_{\mathbf{k}}\ell_{\mathbf{p}})^2 \frac{B_{\mathbf{p}}(V^{(2)}_{\mathbf{k},\mathbf{p},\mathbf{p},\mathbf{k}} + V^{(3)}_{\mathbf{k},\mathbf{p},\mathbf{p},\mathbf{k}})}{2E_{\mathbf{p}}}$$
$$+ \Big(\frac{1}{N}\Big)^2 \sum_{\mathbf{pq}} 2(2\ell_{\mathbf{p}}\ell_{\mathbf{q}}\ell_{\mathbf{k}}\ell_{[\mathbf{k}+\mathbf{p}-\mathbf{q}]})^2 \Big[\frac{V^{(2)}_{\mathbf{k},\mathbf{p},\mathbf{q},[\mathbf{k}+\mathbf{p}-\mathbf{q}]} V^{(3)}_{[\mathbf{k}+\mathbf{p}-\mathbf{q}],\mathbf{q},\mathbf{p},\mathbf{k}}}{\omega - E_{\mathbf{p}} - E_{\mathbf{q}} - E_{[\mathbf{k}+\mathbf{p}-\mathbf{q}]} + i\delta}$$
$$- \frac{V^{(7)}_{\mathbf{k},\mathbf{p},\mathbf{q},[\mathbf{k}+\mathbf{p}-\mathbf{q}]} V^{(8)}_{[\mathbf{k}+\mathbf{p}-\mathbf{q}],\mathbf{q},\mathbf{p},\mathbf{k}}}{\omega + E_{\mathbf{p}} + E_{\mathbf{q}} + E_{[\mathbf{k}+\mathbf{p}-\mathbf{q}]} - i\delta}\Big], \tag{A6a}$$

$$\Sigma^{(2)}_{\alpha\beta}(\mathbf{k},\omega) = \Sigma^{(2)}_{\beta\alpha}(\mathbf{k},\omega) = \Big(\frac{1}{N}\Big)^2 \sum_{\mathbf{pq}} 2(2\ell_{\mathbf{p}}\ell_{\mathbf{q}}\ell_{\mathbf{k}}\ell_{[\mathbf{k}+\mathbf{p}-\mathbf{q}]})^2 \times$$
$$\Big[\frac{V^{(2)}_{\mathbf{k},\mathbf{p},\mathbf{q},[\mathbf{k}+\mathbf{p}-\mathbf{q}]} V^{(7)}_{[\mathbf{k}+\mathbf{p}-\mathbf{q}],\mathbf{q},\mathbf{p},\mathbf{k}}}{\omega - E_{\mathbf{p}} - E_{\mathbf{q}} - E_{[\mathbf{k}+\mathbf{p}-\mathbf{q}]} + i\delta} - \frac{V^{(7)}_{\mathbf{k},\mathbf{p},\mathbf{q},[\mathbf{k}+\mathbf{p}-\mathbf{q}]} V^{(5)}_{[\mathbf{k}+\mathbf{p}-\mathbf{q}],\mathbf{q},\mathbf{p},\mathbf{k}}}{\omega + E_{\mathbf{p}} + E_{\mathbf{q}} + E_{[\mathbf{k}+\mathbf{p}-\mathbf{q}]} - i\delta}\Big], \tag{A6b}$$

where $[\mathbf{k}+\mathbf{p}-\mathbf{q}]$ is meant to be mapped to $(\mathbf{k}+\mathbf{p}-\mathbf{q})$ in the first BZ by an appropriate reciprocal vector $\mathbf{G}$. In deriving Eqs. (A6a) and (A6b) we have used the symmetry properties of the vertices, see Eq. (B3a).

The sublattice magnetization M_s for the A sublattice can be expressed as

$$M_s = S - \langle a_i^{\dagger} a_i \rangle = S - \Delta S + \frac{M_1}{(2S)} + \frac{M_2}{(2S)^2}, \tag{A7}$$

where

$$\Delta S = \frac{1}{N}\sum_{\mathbf{k}} \frac{1}{2\epsilon_{\mathbf{k}}} - \frac{1}{2}, \tag{A8a}$$

$$M_1 = \frac{1}{N}\sum_{\mathbf{k}} \frac{l_{\mathbf{k}} m_{\mathbf{k}} B_{\mathbf{k}}}{E_{\mathbf{k}}}, \tag{A8b}$$

$$M_2 = \frac{1}{N}\sum_{\mathbf{k}} \Big[- (l^2_{\mathbf{k}} + m^2_{\mathbf{k}})\frac{B^2_{\mathbf{k}}}{4E^2_{\mathbf{k}}} + \frac{l_{\mathbf{k}} m_{\mathbf{k}}}{E_{\mathbf{k}}}\Sigma^{(2)}_{\alpha\beta}(\mathbf{k}, -E_{\mathbf{k}})$$
$$- \Big(\frac{1}{N}\Big)^2 \sum_{\mathbf{pq}} 2(2l_{\mathbf{k}} l_{\mathbf{p}} l_{\mathbf{q}} l_{\mathbf{k}+\mathbf{p}-\mathbf{q}})^2 \Big\{ \frac{(l^2_{\mathbf{k}} + m^2_{\mathbf{k}}) V^{(7)}_{\mathbf{k},\mathbf{p},\mathbf{q},[\mathbf{k}+\mathbf{p}-\mathbf{q}]} V^{(8)}_{[\mathbf{k}+\mathbf{p}-\mathbf{q}],\mathbf{q},\mathbf{p},\mathbf{k}}}{(E_{\mathbf{k}} + E_{\mathbf{p}} + E_{\mathbf{q}} + E_{\mathbf{k}+\mathbf{p}-\mathbf{q}})^2}$$
$$+ \frac{2l_{\mathbf{k}} m_{\mathbf{k}} V^{(7)}_{\mathbf{k},\mathbf{p},\mathbf{q},[\mathbf{k}+\mathbf{p}-\mathbf{q}]} V^{(5)}_{[\mathbf{k}+\mathbf{p}-\mathbf{q}],\mathbf{q},\mathbf{p},\mathbf{k}}}{E^2_{\mathbf{k}} - (E_{\mathbf{p}} + E_{\mathbf{q}} + E_{\mathbf{k}+\mathbf{p}-\mathbf{q}})^2} \Big\}\Big]. \tag{A8c}$$

The zeroth-order term ΔS corresponds to the reduction of magnetization within LSWT, M_1 term corresponds to the first-order $1/S$ correction, and M_2 is the second-order correction.

Appendix B: Vertex factors

The vertex factors for the AF-AF and F-AF bilayers required for our calculations are given below.

1. AF-AF Phase

$$\begin{aligned}
V^{(2)}_{12;34} &= \frac{1}{4}\Big[-x_3\gamma(2-3) - x_4\gamma(2-4) - x_1x_2x_3\gamma(1-3) - x_1x_2x_4\gamma(1-4) \\
&\quad + x_1x_2\gamma(1) + \gamma(2) + x_1x_2x_3x_4\gamma(1-3-4) + x_3x_4\gamma(2-3-4)\Big], \qquad \text{(B1a)}\\
V^{(3)}_{12;34} &= \frac{1}{4}\Big[-x_1\gamma(1-3) - x_2\gamma(2-3) - x_1x_3x_4\gamma(1-4) - x_2x_3x_4\gamma(2-4) \\
&\quad + x_1x_3\gamma(1) + x_2x_3\gamma(2) + x_1x_4\gamma(1-3-4) + x_2x_4\gamma(2-3-4)\Big], \qquad \text{(B1b)}\\
V^{(5)}_{12;34} &= \frac{1}{4}\Big[-x_2x_3x_4\gamma(1-3) - x_1x_3x_4\gamma(2-3) - x_1\gamma(2-4) - x_2\gamma(1-4) \\
&\quad + x_1x_4\gamma(2) + x_2x_4\gamma(1) + x_1x_3\gamma(2-3-4) + x_2x_3\gamma(1-3-4)\Big], \qquad \text{(B1c)}\\
V^{(7)}_{12;34} &= \frac{1}{4}\Big[x_1x_4\gamma(1-3) + x_1x_3\gamma(1-4) + x_2x_3\gamma(2-4) + x_2x_4\gamma(2-3) \\
&\quad - x_1x_3x_4\gamma(1) - x_2x_3x_4\gamma(2) - x_1\gamma(1-3-4) - x_2\gamma(2-3-4)\Big], \qquad \text{(B1d)}\\
V^{(8)}_{12;34} &= \frac{1}{4}\Big[x_1x_4\gamma(2-4) + x_2x_4\gamma(1-4) + x_1x_3\gamma(2-3) + x_2x_3\gamma(1-3) \\
&\quad - x_1\gamma(2) - x_2\gamma(1) - x_1x_3x_4\gamma(2-3-4) - x_2x_3x_4\gamma(1-3-4)\Big]. \qquad \text{(B1e)}
\end{aligned}$$

2. F-AF Phase

$$
\begin{aligned}
V^{(2)}_{12;34} = \frac{1}{2}\Big[& -(x_2 + x_1x_3x_4)\{\gamma_1(2-3)+\gamma_1(2-4)+\gamma_1(1-3)+\gamma_1(1-4)\} \\
& + (x_1 + x_2x_3x_4)\{\gamma_1(1)+\gamma_1(4+3-2)\} + (x_2 + x_1x_3x_4)\{\gamma_1(2)+\gamma_1(4+3-1)\}\Big] \\
& + \frac{\eta}{4}\Big[-x_3\gamma_2(2-3) - x_4\gamma_2(2-4) - x_1x_2x_3\gamma_2(1-3) - x_1x_2x_4\gamma_2(1-4) \\
& + x_1x_2\gamma_2(1) + \gamma_2(2) + x_1x_2x_3x_4\gamma_2(4+3-1) + x_3x_4\gamma_2(4+3-2)\Big].
\end{aligned} \tag{B2a}
$$

$$
\begin{aligned}
V^{(3)}_{12;34} = \frac{1}{2}\Big[& -(x_3 + x_1x_2x_4)\{\gamma_1(2-3)+\gamma_1(2-4)+\gamma_1(1-3)+\gamma_1(1-4)\} \\
& + (x_3 + x_1x_2x_4)\{\gamma_1(1)+\gamma_1(2)+\gamma_1(4+3-1)+\gamma_1(4+3-2)\}\Big] \\
& + \frac{\eta}{4}\Big[x_3x_4\gamma_2(2-3) + \gamma_2(2-4) + x_1x_2x_3x_4\gamma_2(1-3) + x_1x_2\gamma_2(1-4) \\
& - x_1x_2x_4\gamma_2(1) - x_4\gamma_2(2) - x_1x_2x_3\gamma_2(4+3-1) - x_3\gamma_2(4+3-2)\Big].
\end{aligned} \tag{B2b}
$$

$$
\begin{aligned}
V^{(5)}_{12;34} = \frac{1}{2}\Big[& -(x_3 + x_1x_2x_4)\{\gamma_1(2-3)+\gamma_1(2-4)+\gamma_1(1-3)+\gamma_1(1-4)\} \\
& + (x_3 + x_1x_2x_4)\{\gamma_1(1)+\gamma_1(2)+\gamma_1(4+3-1)+\gamma_1(4+3-2)\}\Big] \\
& + \frac{\eta}{4}\Big[-x_1x_3x_4\gamma_2(2-3) - x_1\gamma_2(2-4) - x_2x_3x_4\gamma_2(1-3) - x_2\gamma_2(1-4) \\
& + x_2x_4\gamma_2(1) + x_1x_4\gamma_2(2) + x_2x_3\gamma_2(4+3-1) + x_1x_3\gamma_2(4+3-2)\Big].
\end{aligned} \tag{B2c}
$$

$$
\begin{aligned}
V^{(7)}_{12;34} = \frac{1}{2}\Big[& (x_1x_2 + x_3x_4)\{\gamma_1(2-3)+\gamma_1(2-4)+\gamma_1(1-3)+\gamma_1(1-4)\} \\
& - (x_1x_2 + x_3x_4)\{\gamma_1(1)+\gamma_1(2)+\gamma_1(4+3-1)+\gamma_1(4+3-2)\}\Big] \\
& + \frac{\eta}{4}\Big[x_2x_3\{\gamma_2(2-3)+\gamma_2(2-4)\} + x_1x_3\{\gamma_2(1-3)+\gamma_2(1-4)\} \\
& - x_1x_3x_4\gamma_2(1) - x_2x_3x_4\gamma_2(2) - x_1\gamma_2(4+3-1) - x_2\gamma_2(4+3-2)\Big].
\end{aligned} \tag{B2d}
$$

$$
\begin{aligned}
V^{(8)}_{12;34} = \frac{1}{2}\Big[& (x_1x_2 + x_3x_4)\{\gamma_1(2-3)+\gamma_1(2-4)+\gamma_1(1-3)+\gamma_1(1-4)\} \\
& - (x_1x_2 + x_3x_4)\{\gamma_1(1)+\gamma_1(2)+\gamma_1(4+3-1)+\gamma_1(4+3-2)\}\Big] \\
& + \frac{\eta}{4}\Big[x_1x_3\gamma_2(2-3) + x_1x_4\gamma_2(2-4) + x_2x_3\gamma_2(1-3) + x_2x_4\gamma_2(1-4) \\
& - x_2\gamma_2(1) - x_1\gamma_2(2) - x_2x_3x_4\gamma_2(4+3-1) - x_1x_3x_4\gamma_2(4+3-2)\Big].
\end{aligned} \tag{B2e}
$$

Above, $\Phi_G = \exp(i\mathbf{G})$ where $\mathbf{G}$ is the reciprocal lattice vector. These vertex factors fulfill the following symmetry relations

$$V^{(2)}_{12;34} = V^{(2)}_{12;43}; \quad V^{(3)}_{12;34} = V^{(3)}_{21;34}; \quad V^{(5)}_{12;34} = V^{(5)}_{21;34}, \tag{B3a}$$

$$V^{(7)}_{12;34} = V^{(7)}_{21;34} = V^{(7)}_{12;43}; \quad V^{(8)}_{12;34} = V^{(8)}_{21;34} = V^{(8)}_{12;43}. \tag{B3b}$$

If no reciprocal lattice vector is involved in the momentum conservation, i.e., $\mathbf{G} = 0$, there are some additional symmetries

$$V^{(3)}_{12;34} = V^{(5)}_{12;34}; \quad V^{(7)}_{12;34} = V^{(8)}_{12;34}. \tag{B3c}$$

---

[*] majumdak@gvsu.edu

[†] mahanti@pa.msu.edu

[1] P. W. Anderson, Phys. Rev. **86**, 694 (1952).

[2] A. B. Harris, D. Kumar, B. I. Halperin, and P. C. Hohenberg, Phys. Rev. B **3**, 961 (1971).

[3] H. T. Diep, *Frustrated Spin Systems*, 1st ed. (World Scientific, Singapore, 2004).

[4] C. Lacroix, P. Mendels, and F. Mila, *Introduction to Frustrated Magnetism*, 1st ed., Vol. 164 (Springer-Verlag, Berlin, 2011).

[5] K. Majumdar, Phys. Rev. B **82**, 144407 (2010).

[6] K. Majumdar, J. Phys.: Condens. Matter **23**, 046011 (2011).

[7] S. D. Mahanti and T. A. Kaplan, J. Appl. Phys. **69**, 5382 (1991).

[8] M. Zhu, D. Do, C. R. D. Cruz, Z. Dun, H. D. Zhou, S. D. Mahanti, and X. Ke, Phys. Rev. Lett. **113**, 076406 (2014).

[9] M. Zhu, D. Do, C. R. D. Cruz, Z. Dun, J. G. Cheng, H. Goto, Y. Uwatoko, T. Zou, H. D. Zhou, S. D. Mahanti, and X. Ke, (2015), (in press).

[10] S. L. Dudarev, G. A. Botton, S. V. Savrasov, C. J. Humphreys, and A. P. Sutton, Phys. Rev. B **47**, 1505 (1998).

[11] V. I. Anisimov, J. Zaanen, and O. K. Andersen, Phys. Rev. B **44**, 943 (1991).

[12] V. I. Anisimov, I. V. Solovyev, M. A. Korotin, M. T. Czyzyk, and G. A. Sawatzky, Phys. Rev. B **48**, 16929 (1993).

[13] W. Kunnmann, S. L. Placa, L. M. Corliss, J. M. Hastings, and E. Banks, J. Phys. Chem. Solids **29**, 1359 (1968).

[14] M. Drillon, L. Padel, and J. C. Bernier, Physica (Amsterdam) **97B+C**, 380 (1979).

[15] F. J. Dyson, Phys. Rev. **102**, 1217 (1956).

[16] F. J. Dyson, Phys. Rev. **102**, 1230 (1956).

[17] S. V. Maleev, Zh. Eksp. Teor. Fiz. **33**, 1010 (1957).

[18] S. V. Maleev, Sov. Phys. JETP **6**, 776 (1958).

[19] T. Holstein and H. Primakoff, Phys. Rev. B **58**, 1098 (1940).

[20] K. Majumdar, D. Furton, and G. S. Uhrig, Phys. Rev. B **85**, 144420 (2012).

[21] A. Chubukov, E. Gagliano, and C. Balseiro, Phys. Rev. B **45**, 7889 (1992).

[22] G. S. Uhrig and K. Majumdar, Eur. Phys. J. **B86**, 282 (2013).

[23] K. Majumdar, J. Phys.: Condens. Matter **23**, 116004 (2011).

[24] C. M. Canali and M. Wallin, Phys. Rev. B **48**, 3264 (1993).

[25] A. V. Syromyatnikov, J. Phys. C **22**, 216003 (2010).